CHINESE OPTICS LETTERS

Vol. 22, No. 5 | May 2024

Coexistence of noise-like pulse and dark pulse in an Er/Yb co-doped fiber laser

Jing Li (李 婧), Chuncan Wang (王春灿)*, and Peng Wang (王 鹏)

Key Laboratory of All Optical Network and Advanced Telecommunication Network, Ministry of Education, Institute of Lightwave Technology, Beijing Jiaotong University, Beijing 100044, China

*Corresponding author: chcwang@bjtu.edu.cn

Received December 7, 2023 | Accepted January 23, 2024 | Posted Online May 15, 2024

The coexistence of a noise-like pulse (NLP) and a dark pulse was experimentally demonstrated in a net-anomalous dispersion Er/Yb co-doped fiber (EYDF) laser, for the first time, to our knowledge. The cavity was mode-locked by nonlinear polarization rotation (NPR) technique. Meanwhile, a Sagnac loop with a section of polarization-maintaining fiber (PMF) was used as a comb filter to enable multiwavelength pulse operation. When the PMF length was 0.3 m, an asymmetric two-peak spectrum with central wavelengths of 1565.3 and 1594.2 nm was obtained by adjusting polarization controllers (PCs). It is a composite state of NLP and dark pulse due to the cross-phase modulation between the two different wavelength components along orthogonal polarization axes. The two pulses are synchronized with a repetition rate of 7.53 MHz. By adjusting the PC in the Sagnac loop, the spectral ranges of NLPs and dark pulses can be tuned from 1560 to 1577.8 nm and from 1581.8 to 1605.4 nm, respectively. In addition, the pulse characteristics were investigated by incorporating the PMF with different lengths, where the coexistence patterns can be generated when the PMF lengths were 0.2 and 0.3 m. A longer PMF can lead to a narrowband comb filtering, which causes a larger loss and is not favorable for stable operation of the coexistence regime. This fiber laser demonstrates an interesting operation regime and has significant potential for numerous practical applications.

Keywords: coexistence state; mode-locked fiber laser; Sagnac loop; tunable wavelength.
DOI: 10.3788/COL202422.051403

1. Introduction

Multiwavelength passively mode-locked fiber lasers have attracted widespread research attention because of their versatile applications in wavelength-division multiplexing, optical metrology, optical sensing, optical communication, and so on[1–4]. Specifically, dual-wavelength lasers have emerged as key tools for dual-comb spectroscopy, microwave and terahertz signal generation, and pump-probe measurement[5,6]. Moreover, these lasers can service as an ideal platform to explore rich soliton dynamics. So far, various methods have been proposed to achieve dual-wavelength operation, mainly including intracavity loss control[7], and the introduction of cascaded fiber Bragg gratings (FBGs)[8,9] or some artificial comb filters into laser cavities[10–16]. In particular, the incorporation of a comb filter into the cavity has been proven to be an effective solution for suppressing mode competition and achieving stable multiwavelength operation[10]. It can be achieved in different ways, such as the Lyot filter[11], the Mach–Zehnder interferometer[10], the Sagnac loop mirror[12,13], and the grade-index multimode fiber device[14]. In addition, these comb filters can provide great flexibility in adjusting filter bandwidth, central wavelength, and modulation depth[15–17]. By simply changing the fiber length or imposing external physical perturbations on fibers, filters with different transmission spectra can be obtained. Thus, the utilization of comb filters can be a favorable choice for generating tunable dual-wavelength pulses and further exploring novel soliton dynamics.

As is well known, different soliton operating regimes require specific conditions for their formation, generally leading to the generation of identical soliton types at the two central wavelengths of pulses. This phenomenon has been confirmed in various dual-wavelength fiber lasers, including conventional soliton (CS)[11–13], dissipative soliton (DS)[14], dissipative soliton resonance (DSR) pulse[18], and noise-like pulse (NLP)[15] lasers, etc. However, there are relatively few studies on dual-wavelength pulses with the coexistence of diverse pulse patterns, thus arousing increasing research interest. Recently, Mao *et al.* reported the simultaneous generation of CS and DS in an Er-doped fiber (EDF) laser by exploiting chirped FBG and four-port circulator[19]. The coexistence of DS and self-similar pulses, as well as the coexistence of DS and stretched pulses, has been observed

experimentally in two dual-wavelength EDF lasers with near-zero cavity dispersions[20,21]. A composite operation regime of high-order harmonic soliton molecules and rectangular NLP was experimentally generated in a figure-eight EDF laser[22]. Then the coexistence of NLP and high-order harmonic CS was observed in a dual-wavelength mode-locked Tm-doped fiber (TDF) laser with a Lyot filter[23]. Very recently, a heterogeneous pulse pattern of the coexistence of one NLP at 1559 nm and one CS at 1565.8 nm was obtained in a double-cavity EDF laser[24].

However, the aforementioned dual-wavelength fiber lasers with coexistence of distinct operating regimes do not contain a dark pulse. In some long-distance transmission applications, dark pulses as the optical source are more promising than bright solitons because they are less sensitive to background noise, and their broadening rate is almost half that of bright solitons when propagating in the fiber[25,26]. Then a question arises: could different pulse states containing a dark pulse coexist? Recently, bright–dark pulse pairs[27–30] have been reported in some fiber lasers, featuring the coexistence of CS and dark pulse at different central wavelengths. The formation reason can be the cross-phase modulation (XPM) between different wavelengths or two orthogonally polarization axes[27–32]. In addition, a dual-wavelength hybrid step-like and dark pulse was also generated in a Ti:Bi_2Se_3-based EDF laser[28]. These interesting phenomena revealed rich soliton dynamics in the dual-wavelength operating regime. However, to our knowledge, there have been no reports on lasers with the coexistence of NLPs and dark pulses at different central wavelengths.

In this paper, we investigated the coexistence of NLPs and dark pulses in a mode-locked EYDF laser with a Sagnac loop filter and a piece of highly nonlinear fiber (HNLF). The experimental setup of the net-anomalous dispersion mode-locked EYDF laser is presented in Section 2. The NPR technique is used as the artificial saturable absorber (SA). In Section 3, the experimental results of the hybrid pulses with the coexistence of NLPs and dark pulses are presented. Then, by adjusting the PC in the Sagnac loop, the central wavelengths of two peaks can move from 1560 to 1577.8 nm, and from 1581.8 to 1605.4 nm, respectively. In addition, the influence of the length of polarization-maintaining fiber (PMF) in the Sagnac loop filter on the generation of composite states of NLPs and dark pulses is investigated. Finally, Section 4 summarizes the conclusions.

2. Experiment Setup

The proposed mode-locked EYDF laser based on the NPR mode-locking technique is schematically shown in Fig. 1(a). The gain medium is a 4.6-m-long EYDF (Nufern, SM-EYDF-6/125-XP) with a core absorption of 45 dB/m near 1535 nm and pumped by a 3 W multimode laser diode (LD1) at 976 nm through a $(2+1)\times 1$ pump combiner. A 20:80 optical coupler (OC) is used to extract 20% of the pulse power from the cavity. A 3.1-m HNLF with the near-zero negative dispersion at the 1550 nm waveband is used to enhance the nonlinear effect in the cavity. A polarization-dependent isolator (PD-ISO) is used to ensure the unidirectional propagation of pulses in the cavity while combining with two PCs to enable the NPR operation. An optical circulator is used to connect the Sagnac loop filter into the ring cavity. A 2.8-m-long EDF (LIEKKI Er30-4/125) placed in front of the filter is used to balance intracavity losses and further flatten the gain spectrum combined with that of the EYDF. As shown in Fig. 1(b), the intensities of amplified spontaneous emission (ASE) spectrum in the EDF are higher than those in the EYDF on the long-wavelength side. The EDF is pumped by two 976 nm laser diodes (LD2 and LD3) through 976/1550 nm wavelength-division multiplexers (WDMs). The fiber pigtails of the pump combiner and WDM are SM-GDF-6/125 of 1.6 m and OFS980 of 1.6 m, respectively. The other fibers are SMF segments with a total length of ~7.8 m. Therefore, the total cavity length is ~26.57 m and net-cavity dispersion is $-0.173\ \mathrm{ps}^2$. In addition, an optical spectrum analyzer (Deviser AE8600, OSA) is used to measure the output spectra. A photodetector

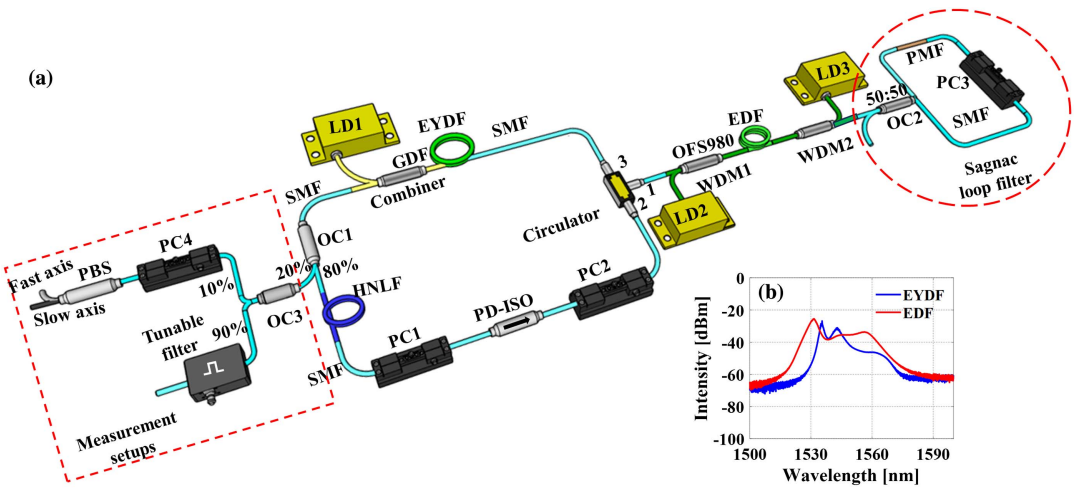

Fig. 1. (a) Schematic diagram of the proposed mode-locked EYDF laser; (b) ASE spectra of EYDF and EDF.

(PD) with the 6-GHz bandwidth together with an electrical spectrum analyzer (Agilent Technologies, N9010A, ESA) and a digital sampling oscillograph (0.3 GHz, Tektronix DPO3032) are employed to monitor the stability of output pulses. The temporal width is evaluated by a commercial optical autocorrelator (FEMTOCHROME, FRXL). A tunable flat-top filter (WL Photonics, WLTF-WM-S/12) with a bandwidth of 12 nm is used to extract the output pulses with tunable central wavelengths. A polarization beam splitter (PBS) is employed to achieve polarization-resolved measurement. Then a 50:50 OC is used to observe pulse waveforms in both temporal and spectral domains simultaneously. P_1, P_2, and P_3 represent the pump powers of LD1, LD2, and LD3, respectively. In order to achieve high output power, P_2 and P_3 are set to the maximum LD power of 0.2 W.

In the experiment, the Sagnac loop filter, acting as a fiber-loop mirror, consists of a 2×2 OC with a splitting ratio of 50:50, a PC, and a 0.3-m-long PMF (YOFC, PM 1550_125/250). The transmission curve of the Sagnac loop filter can be expressed as[33]

$$T = \sin^2\theta \cos^2\left(\frac{\pi \Delta n L_{\mathrm{PMF}}}{\lambda}\right). \tag{1}$$

θ is the rotation angle of the original coordinate system induced by the PC, which determines the amplitude of transmission profile. For simplicity, θ is set to $\pi/2$. The phase difference φ between the fast and slow axes of the PMF can be expressed as $\varphi = \pi \Delta n L_{\mathrm{PMF}}/\lambda$. L_{PMF} is the length of the PMF, and λ is the operating wavelength. The birefringence Δn of the PMF is $\sim 3.5 \times 10^{-4}$, and the wavelength interval between adjacent spectral peaks can be written as

$$\Delta\lambda = \frac{\lambda_0^2}{\Delta n L_{\mathrm{PMF}}}. \tag{2}$$

In this case, $\Delta\lambda$ can be calculated to be ~23 nm, as shown in Fig. 2(a). The experimentally measured transmission spectrum is shown in Fig. 2(b). The interval between two adjacent peaks is 23.2 nm, which is almost consistent with the theoretical value. However, when removing the PMF from the Sagnac loop, no comb-like structure can be observed in the output spectrum.

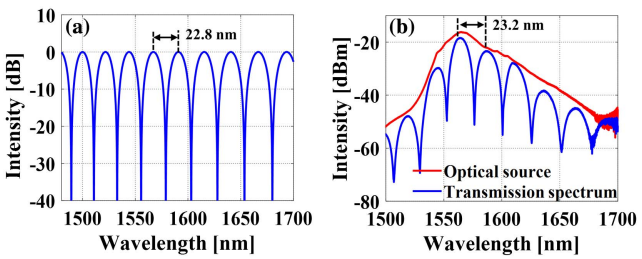

Fig. 2. (a) Calculated spectrum of the Sagnac loop filter when $\theta = \pi/2$, $L_{\mathrm{PMF}} = 0.3$ m; (b) measured transmission spectrum.

3. Results and Discussions

3.1. Coexistence of NLP and dark pulse

When the pump power P_1 was increased to 0.3 W, a mode-locked operation with the two central wavelengths was initiated by appropriately adjusting PCs in the cavity. Furthermore, the stable mode-locked state can remain unchanged as P_1 increased. When P_1 reaches its maximum value of 3 W, Fig. 3(a) shows the two-peak spectrum near 1565.3 and 1594.2 nm, located at two passband windows of the Sagnac loop filter. Since no two-peak pulse spectrum can be observed without a PMF in the Sagnac loop, the periodic transmittance of the filter rather than the intensity-dependent loss induced by NPR effect plays a critical role in a two-peak spectrum. The 3-dB bandwidths of two spectral peaks are 3.5 and 0.7 nm, respectively. The different spectral patterns in two spectral regions can indicate the coexistence of distinct pulse types. The pulse train shown in Fig. 3(b) has a temporal period of ~132.7 ns, which is consistent with the fundamental repetition rate of ~7.53 MHz in Fig. 3(d). As shown in Fig. 3(c), the autocorrelation (AC) curve of the output pulse exhibits a dual-scale structure with a narrow spike riding on a broad pedestal, which is a typical feature of NLP[34,35]. It can further imply the coexistence of an NLP in the laser. A signal-to-noise ratio (SNR) of 64.76 dB suggests the stable operation of the composite state pulses, as shown in Fig. 3(d).

To further investigate the characteristics of the output pulse, a tunable flat-top filter is used to separate the two-peak wavelength components centered at 1565.3 and 1594.2 nm, respectively, as shown in Fig. 4(a). The AC curve of the pulse with blue components exhibits the typical double-scale feature of NLP, as shown in Fig. 4(b). The corresponding pulse train with a temporal interval of 132.7 ns is shown in Fig. 4(c). As shown in Fig. 4(e), it is interesting to note that the output pulse

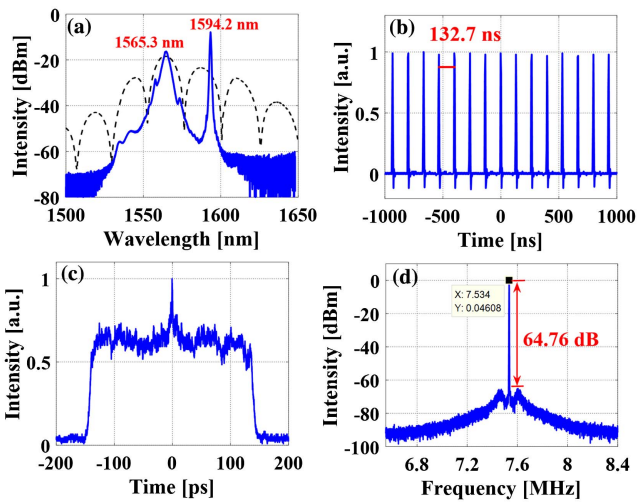

Fig. 3. Output pulse at pump powers of $P_1 = 3$ W, $P_2 = 0.2$ W and $P_3 = 0.2$ W. (a) Pulse spectrum. The black dashed line represents the transmission spectrum of the filter. (b) Oscilloscope pulse trace; (c) normalized AC trace; (d) measured RF spectrum around the fundamental repetition rate of ~7.53 MHz.

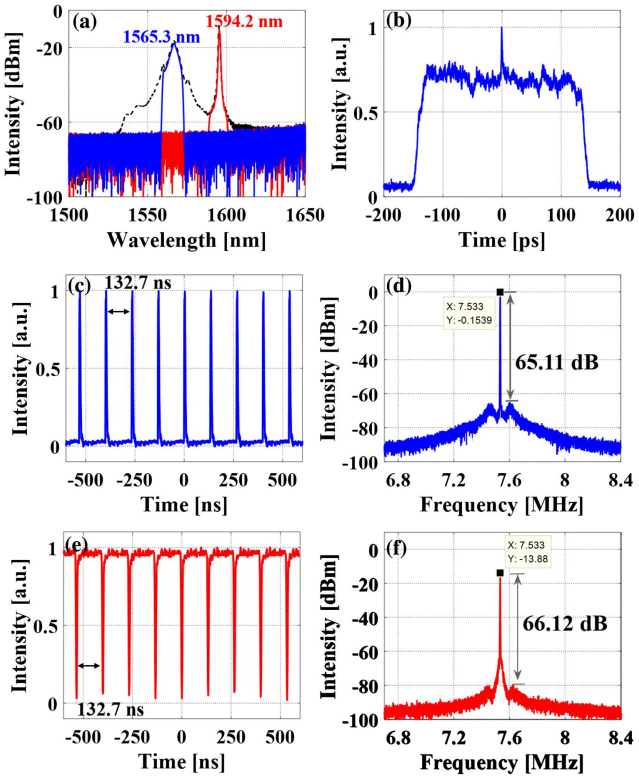

Fig. 4. (a) Individual spectra at 1565.3 and 1594.2 nm, filtered by the tunable flat-top filter; (b) normalized AC trace at 1565.3 nm; oscilloscope pulse traces at (c) 1565.3 nm and (e) 1594.2 nm; measured RF spectra at (d) 1565.3 nm and (f) 1594.2 nm.

corresponding to the 1594.2-nm components exhibits a dip in the continuous-wave (CW) background; hence the name, dark pulses[26,36]. Visualization 1 shows the dynamic evolution of filtered pulses via the oscilloscope and the OSA. First, the dark pulse train appears in the oscilloscope when the central wavelength (λ_f) of the tunable filter is 1594.2 nm. As λ_f shifts toward shorter wavelengths, the amplitudes of both the dip and the CW background decrease, leading to an unstable state when λ_f reaches the dip between two spectral peaks. As λ_f further decreases, the temporal intensity peak gradually emerges on the CW background, and the peak can reach its maximum value when λ_f is 1565.3 nm. Consequently, the coexistence of different types of pulses is obtained in our proposed fiber laser, featuring an NLP on the blue side and a dark pulse on the red side. As shown in Visualization 1, the peak amplitude of the NLP is much larger than that of the dark pulse, which results in an unobvious dark pulse trace in the composite state [see Fig. 3(b)]. In addition, in both two cases, SNRs above 65 dB indicate their stable operations.

Furthermore, the polarization characteristics of the output pulse are investigated via polarization-resolved measurement using an extracavity PBS and a PC4. By finely adjusting the PC4, linearly polarized NLP and dark pulse can be individually observed at the two output ends of the PBS, whose oscilloscope pulse traces are depicted in Fig. 5(a). Obviously, the NLP and the

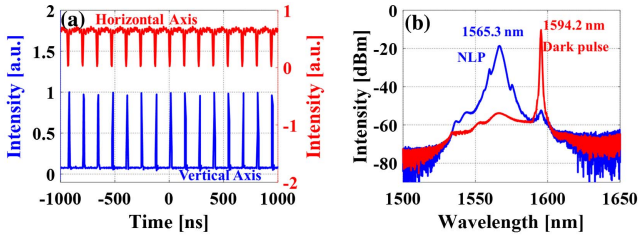

Fig. 5. Polarization-resolved measurement of the coexistence of NLP and dark pulse. (a) Oscilloscope pulse traces of NLP (blue line) and dark pulse (red line) along two orthogonal polarization axes; (b) corresponding spectra.

dark pulse trains have the same temporal interval of ~132.7 ns, indicating that two pulses are synchronized in the laser cavity. The corresponding spectra are shown in Fig. 5(b). The dark pulse is located on the long-wavelength side of the dual-peak spectrum, while the NLP is located on the short-wavelength side. Consequently, the formation of the composite state of NLP and dark pulse can be attributed to the XPM between the two different wavelength components along two orthogonal polarization axes[27,31].

The evolutions of average output power and pulse energy with the pump power P_1 are plotted in Fig. 6(a). Clearly, as P_1 increases from 0.3 to 3 W, the output power linearly increases from 17.8 to 74.7 mW, and the pulse energy increases from 2.37 to 9.93 nJ. Moreover, the stability of output power is measured within 4 h when P_1 is 3 W, as shown in Fig. 6(b). The power fluctuation from the average value is ~1.85%, indicating that the EYDF laser can operate at stable state for a long time in the lab.

3.2. Switchable pulse operations with different states

First, by carefully adjusting the PC in the Sagnac loop filter, wavelength-tunable coexistence states of NLPs and dark pulses are obtained when P_1 is 3 W, as shown in Fig. 7(a). The spectral peak on the blue side can be shifted from 1560 to 1577.8 nm, while the spectral peak on the red side can be tuned from 1581.8 to 1605.4 nm. Both central peaks vary within a range of less than 24 nm due to the limited gain bandwidth of the active fibers. Moreover, the wavelength intervals between two spectral peaks for the curves 1, 2, 3, 4, and 5 are 21.8, 27.5, 34.2, 32.9, and 27.6 nm, respectively. The uneven interval is related to the gain

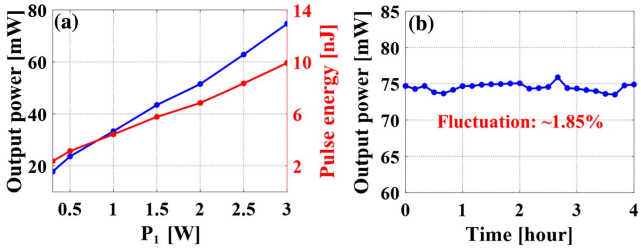

Fig. 6. (a) Average output power and pulse energy with the pump power P_1; (b) power stability in 4 h when $P_1 = 3$ W, $P_2 = 0.2$ W, and $P_3 = 0.2$ W.

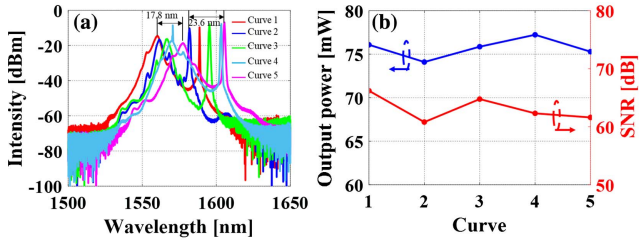

Fig. 7. (a) Output spectra of composite pulses with different central wavelengths, when $P_1 = 3$ W, $P_2 = 0.2$ W, and $P_3 = 0.2$ W; (b) average output powers and SNRs for five spectral curves.

competition between various wavelength components located at the periodic transmittance windows of the filter. As shown in Fig. 7(b), the average output power varies between 74.1 and 77.23 mW. The SNRs of >60 dB indicate that the fiber laser can operate stably at different wavelengths.

Moreover, by keeping P_1 fixed and carefully adjusting the PCs in the main cavity, the state of the fiber laser can be switched from the coexistence regime to the NLP regime. As shown in Fig. 8(a), NLPs with three distinct spectral shapes are generated due to variations in the transmission curve of the NPR-based SA by tuning PCs[37,38]. Notably, the spectrum of the blue trace exhibits the widest 20-dB bandwidth of ~101.4 nm, which corresponds to the narrowest NLP with a pedestal duration (t_0) of ~37.6 ps, shown in Fig. 8(b). Meanwhile, the highest average peak power ($P_{peak} = P_{ave}/f_{repetition\ rate}t_0$) of ~286.6 W is obtained for this broadband NLP due to the nearly identical average output powers (P_{ave}) of 74.3, 75.6, and 74.8 mW in three cases. The reason for the above phenomena is mainly due to the higher critical saturation power (CSP) of the SA obtained in this scenario. It has been demonstrated that the CSP is the key factor directly linked to the properties of NLPs, and a higher value of the CSP allows for NLPs with higher peak power and shorter pulse duration[38]. Consequently, the corresponding spectrum significantly broadens due to the enhanced self-phase modulation effect.

3.3. Influence of the PMF length on composite state pulses

When the length of PMF in the Sagnac loop filter increases from 0.2 to 2.3 m, the channel spacing $\Delta\lambda$ of the filter decreases from 34.3 to 2.9 nm, as shown in Fig. 9. Meanwhile, the transmission spectrum exhibits a more uniform distribution accompanied by a narrower channel bandwidth in the wavelength range of 1550 to 1590 nm. The results are consistent with those in Ref. [39].

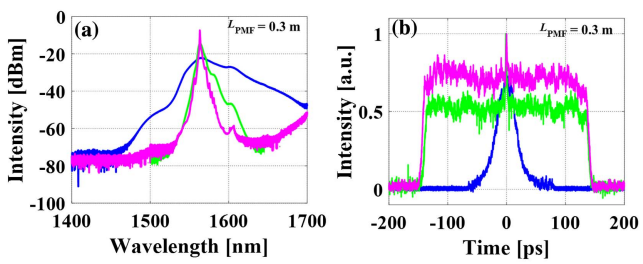

Fig. 8. (a) Output spectra of single-wavelength pulses obtained by adjusting PCs in the main cavity, when $P_1 = 3$ W, $P_2 = 0.2$ W, and $P_3 = 0.2$ W; (b) corresponding normalized AC traces.

First, as shown in Fig. 10(a), switchable coexistence states with two spectral peak tuning ranges of 1560 to 1563.4 nm and 1586.5 to 1602.3 nm are obtained by carefully adjusting PCs when L_{PMF} is 0.2 m and P_1 is 3 W. Evidently, the wavelength variation ranges observed here are relatively smaller than those in the case of $L_{PMF} = 0.3$ m. This result can be attributed to the reduced number of comb channels in the limited gain spectral bandwidth, which imposes certain constraints on the flexible adjustment of the central wavelengths. For example, when $L_{PMF} = 0.2$ m and $L_{PMF} = 0.3$ m, two and three comb channels exist in the wavelength range of 1553 to 1626 nm, respectively, as shown in Fig. 9(a). Similarly, the NLPs with three different spectral curves are also generated, as shown in Fig. 10(b).

However, when L_{PMF} reaches and exceeds 0.5 m, as shown in Fig. 10(c), the laser no longer operates in the composite mode-locked regime, but only in the broadband NLP state. The reason for the disappearance of the coexistence of NLPs and dark pulses

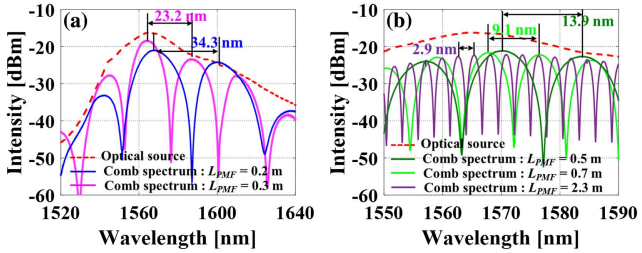

Fig. 9. Transmission spectra of comb filters when PMF lengths are (a) 0.2 and 0.3 m, and (b) 0.5, 0.7, and 2.3 m.

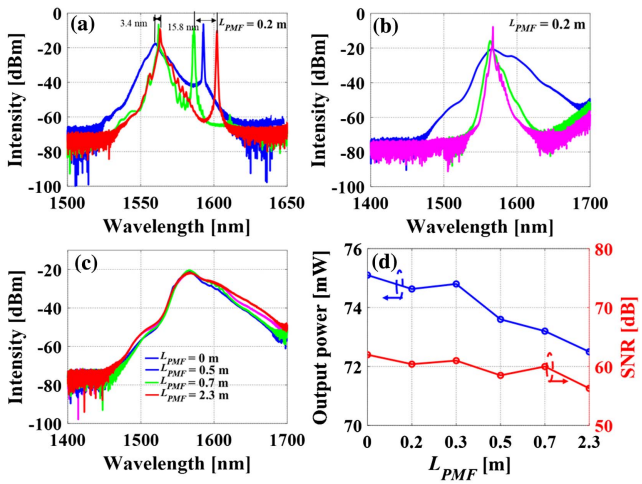

Fig. 10. Output spectra with different L_{PMF} when P_1 is 3 W. (a) Switchable spectra of coexistence states of NLPs and dark pulses and (b) switchable NLP spectra when L_{PMF} is 0.2 m; (c) output spectra of pulses when L_{PMF} are 0, 0.5, 0.7, and 2.3 m; (d) average output powers and SNRs of broadband NLPs with different L_{PMF}.

in our laser is as follows: as L_{PMF} increases, $\Delta\lambda$ decreases, leading to an increased number of channels with reduced channel bandwidth within the limited gain spectral range. Since EYDF and EDF are homogeneous gain mediums[39–41], gain competition becomes stronger with the increased number of channels. As a result, it is difficult to balance gain and loss simultaneously at multiple wavelengths, especially for synchronized pulses with different pulse operation regimes and wavelengths[42]. On the other hand, the losses of wavelength components in each channel increase as the channel bandwidth narrows. Consequently, the intensities of lasing wavelength components decrease and fail to reach the mode-locking threshold power of the NPR-based EYDF laser. Therefore, an SA with a low saturation power and a wide operational wavelength bandwidth is required to initiate a multiwavelength mode-locked operation. For example, by introducing a semiconductor SA mirror into an NPR-based EDF laser with a 1.6-m-long PMF as a Lyot filter, multiwavelength solitons can be generated[43].

Similarly, as losses induced by spectral filtering increase with channel number, only the wavelength components near the peak of the gain spectrum at ~1564 nm have sufficient gains to bleach the NPR-based SA. As a result, the laser can only be operated in the broadband NLP state characterized by a narrow duration and a high average peak power, as shown in Fig. 10(c). In addition, the average output power of the broadband NLP slightly decreases as L_{PMF} increases, as shown in Fig. 10(d). The SNRs of >60 dB indicate the stable operation states of broadband NLPs under different PMF lengths. Nevertheless, it should be noted that the stable NLP operation can only be maintained for ~10 min in the case of $L_{PMF} = 2.3$ m, mainly due to the strong spectral filtering effect induced by the comb-like filter. Therefore, to obtain the coexistence of NLPs and dark pulses and expand their wavelength-tunable range, it is necessary to select an appropriate length of PMF in the Sagnac loop.

4. Conclusion

In conclusion, the coexistence of an NLP and a dark pulse with different central wavelengths was experimentally demonstrated in a net-anomalous dispersion NPR-based EYDF laser for the first time. Via external cavity filtering and polarization-resolved measurements, it has been demonstrated that the composite state is a result of the XPM between the NLP and dark pulse along two orthogonal polarization axes. Moreover, by adjusting the PC in the Sagnac filter, the output pulses exhibit two tunable central wavelengths from 1560 to 1577.8 nm and 1581.8 to 1605.4 nm, respectively. The single-wavelength NLPs with three distinct spectral shapes could also be generated by tuning PCs in the main cavity. Furthermore, the influence of PMF length on composite pulses was investigated. The coexistence states of NLPs and dark pulses were observed only when L_{PMF} were 0.2 and 0.3 m, where the maximum wavelength-tunable range was achieved when $L_{PMF} = 0.3$ m. With a further increase in L_{PMF}, composite states of NLPs and dark pulses disappeared in our fiber laser.

Acknowledgements

This work was supported by the National Natural Science Foundation of China (NSFC) (No. 61575018).

References

1. Z. W. Xu and Z. X. Zhang, "All-normal-dispersion multi-wavelength dissipative soliton Yb-doped fiber laser," Laser Phys. Lett. **10**, 085105 (2013).
2. B. J. Puttnam, G. Rademacher, and R. Luís, "Space-division multiplexing for optical fiber communications," Optica **8**, 1186 (2021).
3. M. G. Xu, J.-L. Archambault, L. Reekie, *et al.*, "Discrimination between strain and temperature effects using dual-wavelength fibre grating sensors," Electron. Lett. **30**, 1085 (1994).
4. F. Ganikhanov, S. Carrasco, X. Xie, *et al.*, "Broadly tunable dual-wavelength light source for coherent anti-Stokes Raman scattering microscopy," Opt. Lett. **31**, 1292 (2006).
5. N. Hoghooghi, R. J. Wright, A. Makowiecki, *et al.*, "Broadband coherent cavity-enhanced dual-comb spectroscopy," Optica **6**, 28 (2019).
6. H. Ahmad, F. D. Muhammad, C. H. Pua, *et al.*, "Dual-wavelength fiber lasers for the optical generation of microwave and terahertz radiation," IEEE J. Sel. Top. Quantum Electron. **20**, 166 (2014).
7. T. Zhu, Z. Wang, D. Wang, *et al.*, "Generation of wavelength-tunable and coherent dual-wavelength solitons in the C + L band by controlling the intracavity loss," Photonics Res. **7**, 853 (2019).
8. C. Zhao, X. Fang, C. Lu, *et al.*, "Switchable multi-wavelength erbium-doped fiber lasers by using cascaded fiber Bragg gratings written in high birefringence fiber," Opt. Commun. **230**, 313 (2004).
9. A. P. Luo, Z. C. Luo, and W. C. Xu, "Switchable dual-wavelength passively mode-locked fiber ring laser using SESAM and cascaded fiber Bragg gratings," Laser Phys. **21**, 395 (2011).
10. A. Jasim and H. Ahmad, "A highly stable and switchable dual-wavelength laser using coupled microfiber Mach–Zehnder interferometer as an optical filter," Opt. Laser Technol. **97**, 12 (2017).
11. Y. Zhu, Z. Cui, X. Sun, *et al.*, "Fiber-based dynamically tunable Lyot filter for dual-wavelength and tunable single-wavelength mode-locking of fiber lasers," Opt. Express **28**, 27250 (2020).
12. R. Li, H. Shi, H. Tian, *et al.*, "All-polarization-maintaining dual-wavelength mode-locked fiber laser based on Sagnac loop filter," Opt. Express **26**, 28302 (2018).
13. X. Luo, T. Tuan, T. Saini, *et al.*, "Switchable dual-wavelength mode-locked fiber laser using Sagnac loop mirror," Opt. Commun. **463**, 125457 (2020).
14. S. Thulasi and S. Sivabalan, "Dual wavelength generation and wavelength tunability in Yb-doped mode-locked laser using few-mode fiber as a saturable absorber," Infrared Phys. Technol. **127**, 104409 (2022).
15. B. Zhang, X. Chen, M. Li, *et al.*, "Single- and dual-wavelength noise-like pulses generation in a Nd-doped all-fiber ring laser based on nonlinear polarization rotation," Infrared Phys. Technol. **116**, 103744 (2021).
16. I. Armas-Rivera, L. A. Rodriguez-Morales, M. Durán-Sánchez, *et al.*, "Wide wavelength-tunable passive mode-locked Erbium-doped fiber laser with a SESAM," Opt. Laser Technol. **134**, 106593 (2021).
17. Y. S. Fedotov, S. M. Kobtsev, R. N. Arif, *et al.*, "Spectrum-, pulsewidth-, and wavelength-switchable all-fiber mode-locked Yb laser with fiber based birefringent filter," Opt. Express **20**, 17797 (2012).
18. P. Wang, K. Zhao, X. Xiao, *et al.*, "Pulse dynamics of dual-wavelength dissipative soliton resonances and switchable domain wall solitons in a Tm fiber laser with fiber-based Lyot filter," Opt. Express **25**, 30708 (2017).
19. D. Mao, X. Liu, D. Han, *et al.*, "Compact all-fiber laser delivering conventional and dissipative solitons," Opt. Lett. **38**, 3190 (2013).
20. X. Li, S. Dai, W. Zou, *et al.*, "Simultaneous emission of Gaussian-like and parabolic-like pulse waveforms in an erbium-doped dual-wavelength fiber laser," Sci. Rep. **7**, 9414 (2017).
21. X. Jin, M. Zhang, G. Hu, *et al.*, "Broad bandwidth dual-wavelength fiber laser simultaneously delivering stretched pulse and dissipative soliton," Opt. Express **28**, 6937 (2020).
22. Y. Huang, Z. Hu, H. Cui, *et al.*, "Coexistence of harmonic soliton molecules and rectangular noise-like pulses in a figure-eight fiber laser," Opt. Lett. **41**, 4056 (2016).

23. Y. Wang, J. Li, E. Zhang, *et al.*, "Coexistence of noise-like pulse and high repetition rate harmonic mode-locking in a dual-wavelength mode-locked Tm-doped fiber laser," Opt. Express **25**, 17192 (2017).
24. L. Gu, Z. Cui, Y. Shu, *et al.*, "Switchable generation of dual-wavelength homogeneous and heterogeneous pulse patterns in a double-cavity fiber laser," Infrared Phys. Technol. **121**, 104042 (2022).
25. Z. C. Tiu, S. W. Harun, H. Ahmad, *et al.*, "Review: dark pulse generation in fiber laser system," Opt. Laser Technol. **151**, 108056 (2022).
26. S. Yang, Q.-Y. Zhang, Z. W. Zhu, *et al.*, "Recent advances and challenges on dark solitons in fiber lasers," Opt. Laser Technol. **152**, 108116 (2022).
27. Q. Y. Ning, S. K. Wang, A. P. Luo, *et al.*, "Bright-dark pulse pair in a figure-eight dispersion-managed passively mode-locked fiber laser," IEEE Photonics J. **4**, 1647 (2012).
28. B. Guo, Y. Yao, J. J. Xiao, *et al.*, "Topological insulator-assisted dual-wavelength fiber laser delivering versatile pulse patterns," IEEE J. Sel. Top. Quantum Electron. **22**, 0900108 (2016).
29. G. D. Shao, Y. F. Song, L. M. Zhao, *et al.*, "Soliton-dark pulse pair formation in birefringent cavity fiber lasers through cross phase coupling," Opt. Express **23**, 26252 (2015).
30. X. Hu, J. Guo, G. D. Shao, *et al.*, "Dissipative dark-bright vector solitons in fiber lasers," Phys. Rev. A **101**, 063807 (2020).
31. G. P. Agrawal, *Nonlinear Fiber Optics*, 5th ed. (Academic, 2013).
32. Y. Song, X. Shi, C. Wu, *et al.*, "Recent progress of study on optical solitons in fiber laser," Appl. Phys. Rev. **6**, 021313 (2019).
33. M. A. Mirza and G. Stewart, "Theory and design of a simple tunable Sagnac loop filter for multiwavelength fiber lasers," Appl. Opt. **47**, 5242 (2008).
34. M. Horowitz, Y. Barad, and Y. Silberberg, "Noise-like pulses with a broadband spectrum generated from an erbium-doped fiber laser," Opt. Lett. **22**, 799 (1997).
35. J. Li, C. Wang, and P. Wang, "Tunable noise-like pulse and *Q*-switched erbium-doped fiber laser," Opt. Express **30**, 4768 (2022).
36. D. Y. Tang, J. Guo, Y. F. Song, *et al.*, "Dark soliton fiber lasers," Opt. Express **22**, 19831 (2014).
37. Y. Jeong, L. A. Vazquez-Zuniga, S. Lee, *et al.*, "On the formation of noise-like pulses in fiber ring cavity configurations," Opt. Fiber Technol. **20**, 575 (2014).
38. O. Pottiez, R. Grajales-Coutiño, B. Ibarra-Escamilla, *et al.*, "Adjustable noise-like pulses from a figure-eight fiber laser," Appl. Opt. **50**, E24 (2011).
39. A. H. Sulaiman, N. M. Yusoff, S. Hitam, *et al.*, "Investigation of continuously adjustable extinction ratio in a multiwavelength SOA fiber laser based on intensity dependent transmission effect," in *IEEE 4th International Conference on Photonics (ICP)* (2013), p. 151.
40. S. Pan, C. Lou, and Y. Gao, "Multiwavelength erbium-doped fiber laser based on inhomogeneous loss mechanism by use of a highly nonlinear fiber and a Fabry-Perot filter," Opt. Express **14**, 1113 (2006).
41. J. D. Filoteo-Razo, J. C. Hernandez-Garcia, J. M. Estudillo-Ayala, *et al.*, "Multi-wavelength Er–Yb-doped fibre ring laser using a double-pass Mach-Zehnder interferometer with a Sagnac interferometer," Opt. Laser Technol. **139**, 106994 (2021).
42. D. Mao, H. Wang, H. Zhang, *et al.*, "Synchronized multi-wavelength soliton fiber laser via intracavity group delay modulation," Nat. Commun. **12**, 6712 (2021).
43. Z. C. Luo, A. P. Luo, and W. C. Xu, "Tunable and switchable multiwavelength passively mode-locked fiber laser based on SESAM and inline birefringence comb filter," IEEE Photonics J. **3**, 64 (2010).